

Unification of valley and anomalous Hall effects in a strained lattice

Jiale Yuan,¹ Han Cai¹, Congjun Wu,^{2,3} Shi-Yao Zhu,¹ Ren-Bao Liu,⁴ and Da-Wei Wang^{1,5,*}

¹Interdisciplinary Center for Quantum Information and State Key Laboratory of Modern Optical Instrumentation, Zhejiang Province Key Laboratory of Quantum Technology and Device and Department of Physics, Zhejiang University, Hangzhou 310027, China

²School of Science, Westlake University, Hangzhou 310024, China

³Key Laboratory for Quantum Materials of Zhejiang Province, School of Science, Westlake University, Hangzhou 310024, China

⁴Department of Physics, Centre for Quantum Coherence, and The Hong Kong Institute of Quantum Information Science and Technology, The Chinese University of Hong Kong, Shatin, New Territories, Hong Kong, China

⁵CAS Center for Excellence in Topological Quantum Computation, University of Chinese Academy of Sciences, Beijing 100190, China

 (Received 8 March 2021; revised 25 June 2021; accepted 29 June 2021; published 9 July 2021)

Two-dimensional lattices are an important stage for studying many aspects of quantum physics, in particular the topological phases. The valley Hall and anomalous Hall effects are two representative topological phenomena. Here we show that they can be unified in a strained honeycomb lattice, where the hopping strengths between neighboring sites are designed by mimicking those between the Fock states in a three-mode Jaynes-Cummings model. Such a strain induces an effective magnetic field, which results in quantized Landau levels. The eigenstates in the zeroth Landau level can be represented by the eigenstates of a large pseudo-spin. We find that the valley Hall current and the chiral edge current in the Haldane model correspond to the pseudo-spin precession around different axes. Our study sheds light on connection between seemingly unrelated topological phases in condensed matter physics.

DOI: [10.1103/PhysRevB.104.035410](https://doi.org/10.1103/PhysRevB.104.035410)

I. INTRODUCTION

Lattice dynamics beyond real space has been investigated in cold atoms [1] and photonic systems [2,3] with synthetic extra dimensions. By using the Fock states of multiple cavities coupled to a two-level atom, lattices in arbitrary dimensions can be synthesized [4–7]. These Fock-state lattices offer a new tool for engineering quantum states (such as the preparation of mesoscopic superposition states [6]) and investigating high-dimensional topological physics [7]. In particular, the inhomogeneous coupling strengths between the Fock states, which are proportional to \sqrt{n} with n being the photon number in the Fock states, resemble strain in real-space lattices. Such a specific strain creates unconventional edges and provides a unique platform for investigating exotic phenomena in strained lattices [8–16].

In graphene, a nonuniform strain can induce an effective magnetic field with a strength much larger than that of a real magnetic field [17–21]. Similar mechanisms have been implemented in atomic and molecular [22,23], photonic [24], and phononic [25,26] lattices to achieve quantized Landau levels. The strain induced magnetic field has opposite signs in the two valleys of graphene, which offers new controlling knobs for valleytronic engineering [27–32]. However, only excitations near the two valleys in weak strain field can be investigated with perturbative methods [9,12,19]. The relation between the two valleys under the same strain, in particular for those that can open a band gap [13], is still unclear.

In this paper, by mimicking the exactly solvable Fock-state lattices, we unify the valley Hall current [33–35] and the chiral

edge current of the Haldane model [36] in a strained tight-binding lattice. The strain results in quantized Landau levels. We use the eigenstates in the zeroth Landau level to construct a large pseudo-spin. The valley Hall current and the chiral edge current correspond to the spin precession about different axes. We also establish a mapping between the Aharonov-Bohm (AB) phase of an electron [37] and the Berry phase of a spin [38]. This Letter sheds new light on hidden relations between different topological phenomena in condensed matter physics.

We schematically show the essence of the valley Hall system and the Haldane model in Fig. 1. In a honeycomb lattice where the inversion symmetry is broken, e.g., by different on-site potential of the two sublattices or a nonuniform strain

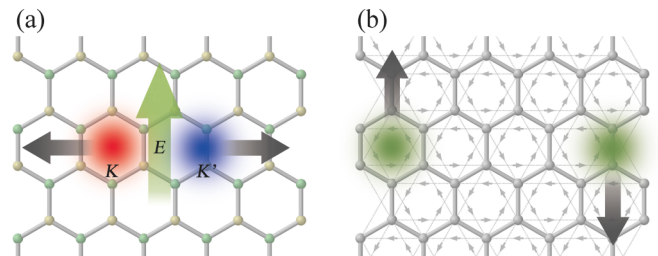


FIG. 1. (a) Valley Hall current. In a honeycomb lattice with inversion symmetry breaking, the two valleys (K and K') have opposite Berry curvatures. Wave packets at the two valleys drift in opposite directions (as shown by the gray arrows) perpendicular to the subjected electric field (the big green arrow). (b) Haldane edge current. With phased next-nearest-neighbor hopping terms (the arrows on the dashed lines show the hopping directions attached with phase factor i) that break the time-reversal symmetry, edge currents propagate in opposite directions (the gray arrows).

*dwwang@zju.edu.cn

field, the Berry curvatures at the two valleys have opposite signs. An electric field would induce Hall currents proportional to the Berry curvatures, such that the wave packets at the two valleys drift in opposite directions [33–35]. On the other hand, in the Haldane model the next-nearest-neighbor (NNN) hopping terms break the time-reversal symmetry and the wave packets propagate in opposite directions at the two edges [36,39,40]. There is a dual relation between the electric field in the valley Hall system and the NNN terms in the Haldane model. In the valley Hall effect, the electric field breaks the inversion symmetry, and the valley currents at the two time-reversal symmetric points (K and K') are opposite. In the Haldane model, the NNN terms break the time-reversal symmetry, and the resulted chiral edge currents at the inversion symmetric points (upper and lower edges) are opposite. Since the time-reversal symmetry is equivalent to momentum-reversal symmetry, such a dual relation indicates that these two effects are unified in an integrated phase space of position and momentum. We found that both of them can be represented by the precession of a large pseudo-spin. The states at the K and K' points correspond to the pseudo-spin states at the north and south poles of the Bloch sphere. The Haldane edge states correspond to the pseudo-spin coherent states at the equator. The valley Hall current and the Haldane edge current correspond to the spin precession around a pseudo-magnetic field in and perpendicular to the lattice plane, respectively.

II. FOCK-STATE LATTICE AND EFFECTIVE MAGNETIC FIELD

To demonstrate that relation, we construct a tight-binding model of exactly flat bands for arbitrary size of lattices [41–44] by borrowing the coupling strengths in the Fock-state lattice of a multimode Jaynes-Cummings (JC) model [6,7,45],

$$H_{JC} = g \sum_{i=1}^3 (c_i \sigma^+ + \sigma^- c_i^\dagger), \quad (1)$$

where g is the vacuum coupling strength, c_i and c_i^\dagger are the bosonic annihilation and creation operators of the photons in the i th cavity, and $\sigma^+ \equiv |b\rangle\langle a|$ and $\sigma^- \equiv |a\rangle\langle b|$ are the raising and lowering operators of a two-level atom with the excited state $|b\rangle$ and ground state $|a\rangle$. The Fock states with p , q , and r photons and the atom in the state $|b/a\rangle$ are denoted as $|b/a; p, q, r\rangle$. The Hamiltonian H_{JC} conserves the total excitation number $N = p + q + r + (\sigma_z + 1)/2$. The eigenstates and eigenenergies can be obtained by transforming the three photonic modes to a bright mode and two dark modes (see Appendix A). The bright mode couples the two atomic states and results in the $\pm\sqrt{n}$ splitting of the energy levels, while the dark modes contribute to the degeneracy of each energy level [7]. These are in reminiscence of the Landau level quantization of electrons near the Dirac cones in graphene, which can be investigated by mapping the coupling coefficients of the Hamiltonian in Eq. (1) to a strained honeycomb tight-binding model. By replacing the Fock states $|b; p-1, q, r\rangle$ and $|a; p, q, r\rangle$ with lattice sites, we construct a tight-binding lattice Hamiltonian,

$$H = \sum_{pqr} g(\sqrt{p}b_{p-1,jk}^\dagger + \sqrt{q}b_{pq-1k}^\dagger + \sqrt{r}b_{pqr-1}^\dagger)a_{pqr} + \text{H.c.}, \quad (2)$$

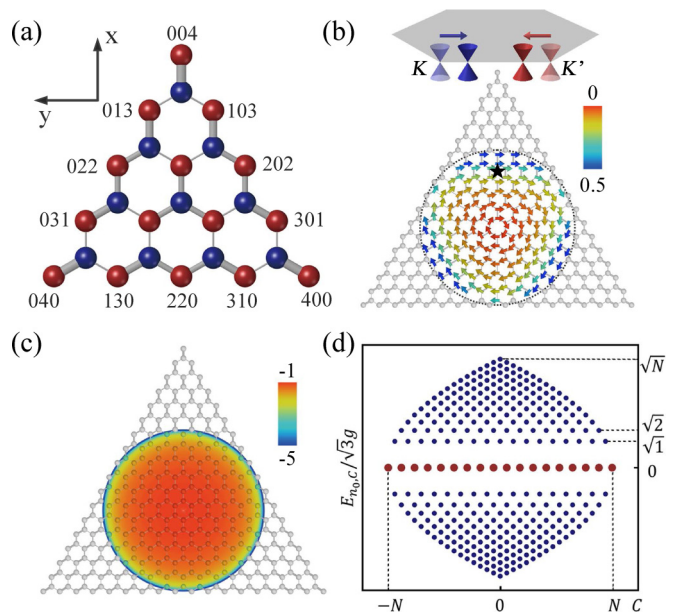


FIG. 2. Effective magnetic field and Landau levels in a tight-binding honeycomb lattice under a JC model strain. (a) A honeycomb tight-binding lattice with Hamiltonian in Eq. (2). Red and blue sites denote a and b sublattices. Numbers label the indices pqr of a -sublattice sites on the boundary. The line widths are proportional to the hopping coefficients. (b) Displacements of the Dirac cones in the Brillouin zone (at the position denoted by “*”) and the distribution of the strain-induced vector potential $A^+(\mathbf{r})/q_0$, where $q_0 = 4\pi/3\sqrt{3}u$. The orientations of the arrows denote the directions and the colors denote the values. (c) Distribution of the strain-induced effective magnetic field $B^+(\mathbf{r})/B_0$. (d) The eigenenergy spectrum of the tight-binding lattice, $E_{n_0,c}^\pm = \pm\sqrt{3}n_0g$ for the upper and lower n_0 th Landau level and chirality C .

where a_{pqr} and b_{pqr} are the fermionic annihilation operators on the two sublattices. The honeycomb lattice contains $(N+1)^2$ sites with a triangular boundary, as shown in Fig. 2(a). We meet the boundary when one of p, q, r becomes zero. We define the center of the triangular boundary as the origin and the x axis pointing at the top vertex and the y axis pointing horizontally to the left, as shown in Fig. 2(a). The coordinates of each site p, q, r are $x = u(2r - p - q)/2$ and $y = \sqrt{3}u(p - q)/2$, with u being the lattice constant, obtained by seeking the expectation values of the operators $x \rightarrow u(2c_3^\dagger c_3 - c_1^\dagger c_1 - c_2^\dagger c_2)/2$ and $y \rightarrow \sqrt{3}u(c_1^\dagger c_1 - c_2^\dagger c_2)/2$ in the corresponding Fock-state lattice. Here “ \rightarrow ” means a mapping to the equivalent quantities in the Fock-state lattice.

In the adiabatic limit, the lowest order Hamiltonian can be expanded near the Dirac points [13,18,46],

$$H = \xi v_F [\mathbf{p} - e\mathbf{A}^\xi(\mathbf{r})] \cdot \sigma, \quad (3)$$

where $v_F = gu\sqrt{3N}/2\hbar$ is the Fermi velocity, $\sigma = \sigma_x \hat{x} + \sigma_y \hat{y}$ is the two-dimensional Pauli matrix vector, \mathbf{p} is the lattice momentum, e is the electric charge, $\mathbf{A}^\xi(\mathbf{r})$ is the strain-induced gauge fields with $\xi = +$ and $-$ for the K and K' points, and \mathbf{r} is the displacement from the geometric center of the lattice. We obtain $\mathbf{A}^\xi(\mathbf{r})$ by calculating the displacements of the two Dirac points due to the strain [9,12,13] [see Fig. 2(b)]. The

strain-induced effective magnetic field is (see Appendix B)

$$\mathbf{B}^\xi(\mathbf{r}) = \nabla \times \mathbf{A}^\xi(\mathbf{r}) = -\xi \frac{B_0}{\sqrt{1 - \mathbf{r}^2/R^2}} \hat{z}, \quad (4)$$

where $B_0 = 2\hbar/Neu^2$, and $R \equiv Nu/2$ is the radius of the incircle of the triangular lattice boundary. By substituting the lattice constant of a real graphene $u = 0.14$ nm, we obtain $B_0 = 6.5 \times 10^4/N$ tesla. For a piece of graphene with micrometer size, N is in the order of 10^4 and B_0 is a few tesla, which is achievable in distorted graphene [19]. Obviously, when $N \rightarrow \infty$, the effective magnetic field at the center of the lattice $B_0 \rightarrow 0$. The effective magnetic field is undefined on the incircle $|\mathbf{r}| = R$ [see Fig. 2(c)], where the two Dirac points merge and a band gap opens [13]. A Lifshitz topological phase transition [47] occurs on the in-circle, which is an unconventional edge that encloses a piece of semimetal in real space and connects the K and K' points in momentum space. Such an edge enables us to integrate the valley Hall system and the Haldane model in a unified picture.

III. RELATION BETWEEN THE BERRY PHASE OF A SPIN AND THE AHARONOV-BOHM PHASE

We diagonalize H in Eq. (2) by borrowing coefficients of the eigenstates of H_{JC} in Eq. (1), which can be easily diagonalized by introducing three combinational modes [6,7], $d_0^\dagger = \sum_j c_j^\dagger/\sqrt{3}$ and $d_\pm^\dagger = \sum_j c_j^\dagger \exp(\pm 2ij\pi/3)/\sqrt{3}$ (see Appendix A), and the eigenenergy spectrum is shown in Fig. 2(d). It is obvious that the eigenenergies scale with \sqrt{n} , the same as the Landau levels of electrons in a magnetic field near the Dirac cones of graphene. There are $N + 1$ zero-energy states, $|\psi_{0,C}\rangle = |a; 0, n_+, n_-\rangle_d$, where $C = n_+ - n_-$ and $n_j = \langle d_j^\dagger d_j \rangle$ in the state ket $|\dots\rangle_d$ is the photon number in the Fock state of the d_j mode ($j = 0, \pm$). By introducing the Schwinger representation of an angular momentum, $J_x = (d_+^\dagger d_- + d_-^\dagger d_+)/2$, $J_y = i(-d_+^\dagger d_- + d_-^\dagger d_+)/2$ and $J_z = (d_+^\dagger d_+ - d_-^\dagger d_-)/2$ [48], we construct the eigenstates of a pseudo-spin $j = N/2$ by using the states $|\psi_{0,2m}\rangle$ with $m = -N/2, -N/2 + 1, \dots, N/2$ being the magnetic quantum numbers. It is interesting to note that J_x and J_y are time-reversal even while J_z is time-reversal odd, which turns out to be responsible for the symmetry properties in the valley and anomalous Hall effects, respectively.

A pseudo-spin coherent state $|\theta, \phi\rangle$ [49,50] (see Appendix C) corresponds to a wave function in the honeycomb lattice, $\psi_{\theta,\phi}(\mathbf{r})$, as shown in Figs. 3(a) and 3(b). We establish the correspondence between the polar coordinates (θ, ϕ) and the position \mathbf{r} by overlapping the equator of the Bloch sphere and the in-circle of the tight-binding lattice, as shown in Fig. 3(c). The expectation value of the position \mathbf{r} of the electronic wave function $\psi_{\theta,\phi}(\mathbf{r})$ is the projection of the Bloch sphere point (θ, ϕ) on the equator plane, i.e., $\langle \mathbf{r} \rangle = R \sin \theta \cos \phi \hat{x} + R \sin \theta \sin \phi \hat{y}$ (see Appendix C). We adiabatically move the state $|\theta, \phi\rangle$ along a small loop that subtends a solid angle $d\Omega$ [see Fig. 3(c)], the accumulated Berry phase is [38,49]

$$d\gamma = -Nd\Omega/2. \quad (5)$$

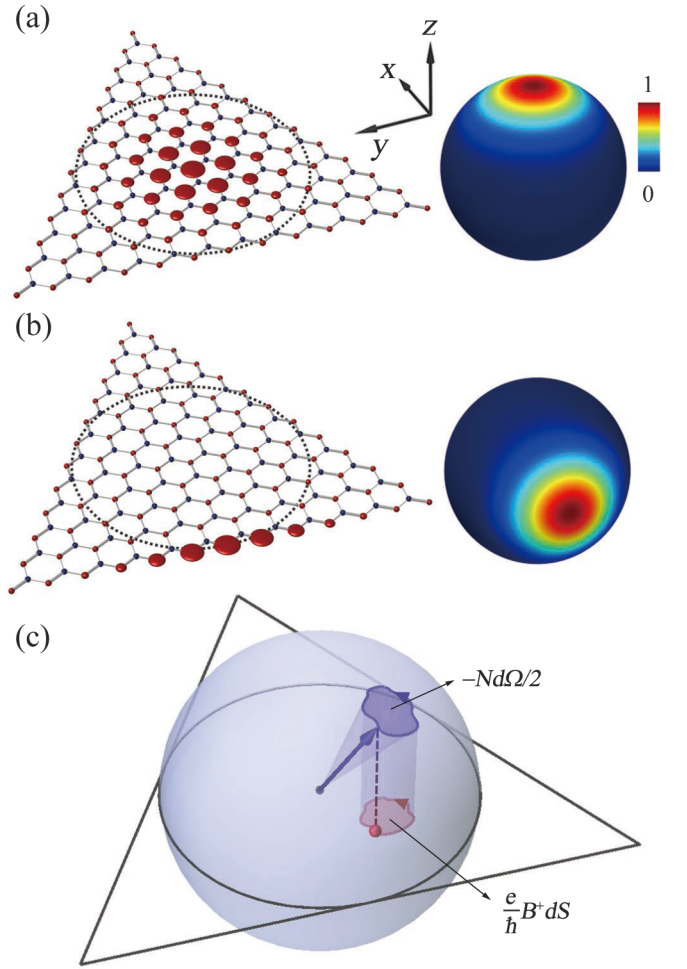


FIG. 3. States and Berry phases in the zeroth Landau level compared with those of a pseudo-spin. Quasidistribution function $W(\theta, \phi) = |\langle \theta', \phi' | \theta, \phi \rangle|^2$ of the spin coherent states $|\theta, \phi\rangle = |0, 0\rangle$ (a) and $|\pi/2, \pi\rangle$ (b) are shown with the probability distributions of the corresponding states $\psi_{\theta,\phi}(\mathbf{r})$ in the zeroth Landau level of the strained lattice. The radii of the filled circles in the lattice are proportional to the probabilities on the corresponding sites. (c) Relation between the Berry phase of the pseudo-spin and the AB phase in the lattice, both accumulated in closed loops.

The mapping between the pseudo-spin coherent state and the wave function ensures that $\psi_{\theta,\phi}(\mathbf{r})$ accumulates the same geometric phase during the adiabatic transport. In this case it is the AB phase,

$$d\gamma = \frac{e}{\hbar} B^\xi dS. \quad (6)$$

We note that $dS = \xi R^2 \cos \theta d\Omega$ with $\xi = +$ and $-$ for projection from the upper and lower halves of the Bloch sphere. By equating Eqs. (5) and (6) we obtain B^ξ in Eq. (4), which can also be calculated independently through the strain induced motion of the Dirac points. These two geometric phases were the two examples given in the original paper of Berry [38]. Here we show that in our specific model the two geometric phases can be mapped into each other. In contrast to a pseudo-spin-1/2 model that is usually used for the two valleys [33],

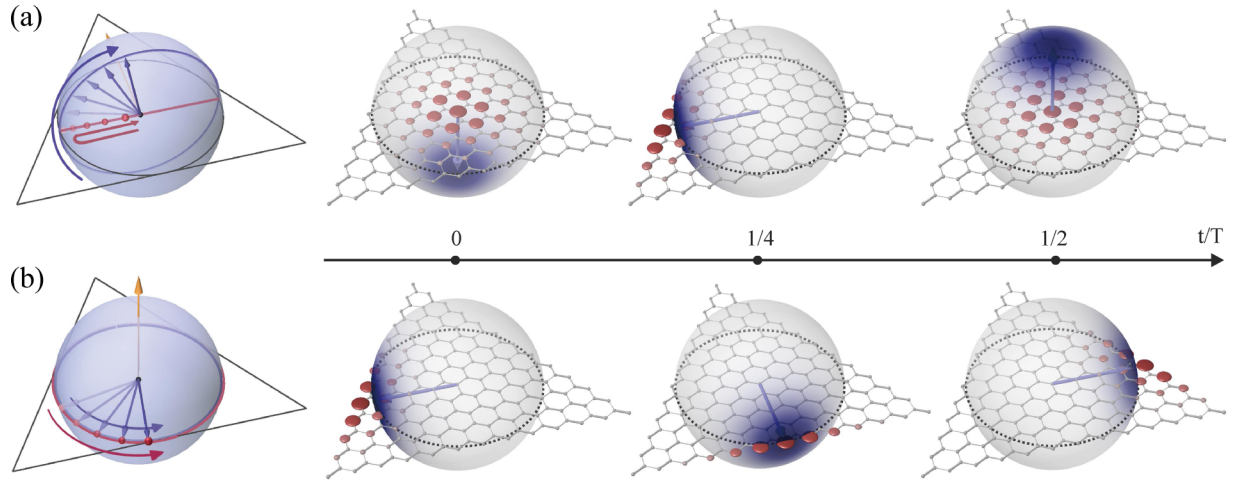


FIG. 4. A unified picture of electronic responses in the valley and anomalous Hall effects. (a) Time evolution of the electronic wave packet in a static electric field in $-x$ direction with the initial state $|\theta, \phi\rangle = |\pi, 0\rangle$. (b) Time evolution of the edge state in the Haldane model with the initial state $|\theta, \phi\rangle = |\pi/2, \pi/2\rangle$. Figures on the left show the traces of the states during the time evolution, with the yellow arrows being the precession axes. The arrows to the Bloch sphere represent the spin coherent states. The curled blue and red arrows show the traces of the spin coherent state and the zeroth Landau level state, respectively. Figures on the right are three snapshots of the states during the evolution in sequence, at $t = 0, T/4$ and $T/2$ with T being the precession period.

here the K and K' points correspond to the two poles of the Bloch sphere of a spin- $N/2$.

IV. RELATION BETWEEN THE VALLEY HALL RESPONSE AND THE CHIRAL EDGE CURRENT IN THE HALDANE MODEL

To investigate the valley Hall effect, we introduce the potential due to a weak electric field $H_V = -eE_x x - eE_y y$. Here the field is weak, i.e., $euE_x, euE_y \ll g$ such that the transition between different Landau levels (i.e., the Landau-Zener tunneling) is negligible. We rewrite x and y in the d modes and drop the terms containing d_0 and d_0^\dagger , which would induce interband transitions. Then we obtain $X = x - P_y/eB^\xi = uJ_x$ and $Y = y + P_x/eB^\xi = uJ_y$, which, containing no d_0 terms, are the x and y coordinates of the guiding center, describing the motion within a Landau level, with P_x and P_y , which contain d_0 terms, denoting the mechanical momenta involving transition between Landau levels [18] (see Appendix D). Consequently, the valley Hall effect can be calculated by the following Hamiltonian,

$$H_V \rightarrow -eu\mathbf{E} \cdot \mathbf{J}. \quad (7)$$

The valley Hall response of the electronic wave function is represented by the precession of a pseudo-spin around a pseudo-magnetic field pointing in the x - y plane. The static electric field in the Hall effect plays the role of a pseudo-magnetic field. Here the pseudo-magnetic field acting on the pseudo-spin (as mapped from the electric field in the lattice) should not be confused with the effective magnetic field due to strain of the lattice.

In the valley Hall effect, the strain-induced effective magnetic fields and thus the Hall responses at the two valleys have opposite signs [19]. We assume that the electric field is applied along the $-x$ direction, and the Hamiltonian is $euE_x J_x$. The

Heisenberg equation of J_y is

$$\dot{J}_y = \frac{1}{i\hbar} [J_y, euE_x J_x] = -\frac{euE_x J_z}{\hbar}. \quad (8)$$

At the K and K' point, $J_z = \xi N/2$, we obtain $\dot{Y} = u\dot{J}_y = -\xi E_x/B_0$, which is evident that the Hall responses at the two valleys have opposite signs, as shown in Fig. 4(a) at $t = 0$ and $T/2$. At the two valleys, the Hall conductivity contributed by the electrons in the zeroth Landau level is (only for one spin),

$$\sigma_{yx}^\xi = \frac{\rho e \dot{Y}}{E_x} = -\xi \frac{e^2}{h}, \quad (9)$$

where $\rho = 1/2\pi l_B^2$ is the density of electrons [18] and $l_B = \sqrt{\hbar/eB}$ is the magnetic length. We have used the relation $l_B/u = \sqrt{N/2}$ at the two valleys [7]. Since the magnetic field depends on the position, the velocity of the electronic wave function changes when it moves, characterized by an oscillation in the in-circle and reflection at the Lifshitz transition edge due to band-gap opening.

We introduce Haldane NNN hopping terms H_H [36,40], e.g., $i\kappa[\sqrt{p(q+1)}a_{(p-1)(q+1)r}^\dagger a_{pqr} - \sqrt{pq}b_{(p-1)qr}^\dagger b_{p(q-1)r}] + \text{H.c.}$ with complex hopping coefficients in the Fock-state lattice,

$$H_H \rightarrow -i\kappa\sigma_z \sum_j c_{j+1}^\dagger c_j + \text{H.c.} = -2\sqrt{3}\kappa\sigma_z J_z, \quad (10)$$

where κ is a coupling coefficient. Therefore, the Haldane terms correspond to a pseudo-magnetic field in z direction and its signs are opposite for the two sublattices. In the zeroth Landau level, only the a sublattice is occupied and $\sigma_z = -1$. The dynamics of the electronic wave function is mapped to the precession of a pseudo-spin in a pseudo-magnetic field pointing in the z direction. A wave packet prepared on the in-circle makes chiral rotation around the center of the lattice, which is the key feature of the Haldane model, as shown in

Fig. 4(b). Although the position-dependent coupling strengths break the translational symmetry of the lattice and the Chern number cannot be calculated from the traditional lattice bands [51], the Chern numbers of the two bands of the Fock-state Haldane model can be obtained from the topological marker [7].

V. DISCUSSION AND CONCLUSION

The results in this paper can be simulated in Fock-state lattices of three resonators coupled to a single qubit in a superconducting circuit [52–54]. The coupling strength g_i between the resonator i and the qubit shall be tunable, such that the initial state can be prepared adiabatically as follows. We first set $g_1 = g_3 = 0$ and g_2 a finite value and prepare an N photon state in resonator 1. We then tune up g_1 to the value of g_2 in a time scale much longer than $1/g_2$ to satisfy the adiabatic condition. In this way we prepare a pseudo-spin coherent state located in the middle of the bottom edge in Fig. 2(a) and the state corresponds to a spin coherent state along $-x$ [7,55]. Then we set $g_3 = g_2$ and detune the frequencies of resonators 1 and 2 to introduce an effective electric field, such that we can observe the valley Hall response by measuring quantum states of the three resonators as functions of time. The Haldane model can be constructed by periodically modulating the frequencies of the three resonators or the three coupling strengths [6,52,56] and the chiral edge current can be observed from the dynamics of the wave function.

In conclusion, we propose an exactly solvable model of a strained lattice whose hopping rates are derived from the transitions between the Fock states of a three-mode JC model. The states in the zeroth Landau level of the strain-induced effective magnetic field can be represented by a pseudo-spin. We demonstrate that the valley Hall current can be represented by the spin precession around an in-plane pseudo-magnetic field, while the chiral edge current in the Haldane model can be represented by the spin precession around a pseudo-magnetic field perpendicular to the lattice plane. The method can be generalized to various strained lattices in arbitrary dimensions by introducing more atomic levels or cavity modes. This work reveals deep connections between the topological phases in condensed matter physics and cavity quantum electrodynamics.

ACKNOWLEDGMENTS

This work was supported by the National Key Research and Development Program of China (Grants No. 2019YFA0308100 and No. 2018YFA0307200), the National Natural Science Foundation of China (Grants No.11934011 and No. 11874322), the Strategic Priority Research Program of Chinese Academy of Sciences (Grant No. XDB28000000), and the Fundamental Research Funds for the Central Universities. H.C. was supported by the China Postdoctoral Science Foundation (Grant No. 2021M692838). R.B.L. was supported by Hong Kong Research Grants Council-General Research Fund Project 14304117. C.W. acknowledges the support from the National Natural Science Foundation of China under the Grant No. 11729402.

APPENDIX A: EIGENSTATES OF THE MULTIMODE JC MODEL

The JC model Hamiltonian in Eq. (1) can be simplified by introducing the mode transformation

$$\begin{bmatrix} d_0^\dagger \\ d_+^\dagger \\ d_-^\dagger \end{bmatrix} = \frac{1}{\sqrt{3}} \begin{bmatrix} 1 & 1 & 1 \\ e^{2i\pi/3} & e^{4i\pi/3} & 1 \\ e^{-2i\pi/3} & e^{-4i\pi/3} & 1 \end{bmatrix} \begin{bmatrix} c_1^\dagger \\ c_2^\dagger \\ c_3^\dagger \end{bmatrix} \equiv U[c_i^\dagger], \quad (\text{A1})$$

where $UU^\dagger = 1$ and $[d_i^\dagger, d_j] = -\delta_{ij}$ for $i, j = 0, +, -$. Then H_{JC} is reduced to a single-mode JC model

$$H_{JC} = \sqrt{3}g(d_0\sigma^+ + d_0^\dagger\sigma^-), \quad (\text{A2})$$

whose eigenstates are $|\psi_{n_0,C}^\pm\rangle = (|b; n_0 - 1, n_+, n_- \rangle_d \pm |a; n_0, n_+, n_- \rangle_d)/\sqrt{2}$ for $n_0 = 1, \dots, N$ with eigenenergy $\pm\sqrt{3n_0}g$ and $|\psi_{0,C}\rangle = |a; n_0, n_+, n_- \rangle_d$ with eigenenergy 0. Here $C = n_+ - n_-$ plays the role of the lattice momentum in an infinite lattice.

For the explicit form of the lattice wave function, we expand $|\psi_{0,C}\rangle$ in the c_j modes to obtain the wave function of the zero energy states,

$$|\psi_{0,C}\rangle = \sum_{pqr} p_{pqr}^C |a; p, q, r\rangle \delta_{N, p+q+r}, \quad (\text{A3})$$

where the coefficients are

$$p_{pqr}^C = \sum_{n_1 n_2 n_3} \frac{\sqrt{n_+! n_-! p! q! r!} e^{i\frac{2\pi}{3}(2n_1 - 2n_2 - p + q)}}{\sqrt{3^N n_1! n_2! n_3! (p - n_1)! (q - n_2)! (r - n_3)!}} \times \delta_{n_+, n_1 + n_2 + n_3}. \quad (\text{A4})$$

The coefficients p_{pqr}^C can be used to construct the eigenmodes in the zeroth Landau level of the tight-binding lattice Hamiltonian H ,

$$\tilde{a}_{0,C}^\dagger = \sum_{pqr} p_{pqr}^C a_{pqr}^\dagger. \quad (\text{A5})$$

Similar procedure can be taken to obtain eigenmodes in other Landau levels of H .

APPENDIX B: EFFECTIVE MAGNETIC FIELD GENERATED BY THE SHIFT OF THE DIRAC CONES

For the Dirac points of a tight-binding honeycomb lattice, the Bloch wave vector \mathbf{p} satisfies the relationship

$$|t_3 + t_1 e^{-i\mathbf{p}\cdot\mathbf{v}_1} + t_2 e^{-i\mathbf{p}\cdot\mathbf{v}_2}| = 0, \quad (\text{B1})$$

where $\mathbf{v}_1 = (-3u/2, \sqrt{3}u/2)$ and $\mathbf{v}_2 = (-3u/2, -\sqrt{3}u/2)$. In the Fock-state lattice the coupling strengths between each a -sublattice site $|a; p, q, r\rangle$ and the three nearest-neighbor b -sublattice sites are $t_1 = \sqrt{q}g$, $t_2 = \sqrt{p}g$, $t_3 = \sqrt{r}g$, correspondingly. Accordingly, the positions of the Dirac points are explicitly obtained through the equations

$$\begin{aligned} \cos \mathbf{p} \cdot \mathbf{v}_2 &= \frac{t_1^2 - t_2^2 - t_3^2}{2t_2 t_3} = \frac{q - p - r}{2\sqrt{pr}} \equiv s_2, \\ \cos \mathbf{p} \cdot \mathbf{v}_1 &= \frac{t_2^2 - t_1^2 - t_3^2}{2t_1 t_3} = \frac{p - q - r}{2\sqrt{qr}} \equiv s_1. \end{aligned} \quad (\text{B2})$$

The above equations only have solutions when $|t_1 - t_2| < t_3 < |t_1 + t_2|$, which results in $p^2 + q^2 + r^2 < N^2/2$, corresponding to sites within the in-circle of the lattice. The sites that cannot satisfy this relation locate outside of the in-circle, where a band gap opens and no Dirac point can be found. The solutions give the position of Dirac points

$$\begin{aligned} p_x^\xi &= \frac{\xi}{3u} (\arccos s_1 - \arccos s_2), \\ p_y^\xi &= -\frac{\xi}{\sqrt{3}u} (\arccos s_1 + \arccos s_2), \end{aligned} \quad (\text{B3})$$

where the superscript ξ in $\mathbf{p}^\xi = (p_x^\xi, p_y^\xi)$ denotes the two Dirac points K (for $\xi = +$) and K' (for $\xi = -$). At the center of the lattice $p = q = r = N/3$, $s_1 = s_2 = -1/2$ and $p_{x0}^\xi = 0$, $p_{y0}^\xi = -\xi 4\pi/3\sqrt{3}u$ are the locations of the unshifted Dirac points at the Brillouin zone corners. Away from the lattice center, the shift of the Dirac points in the Brillouin-zone is equivalent to a vector potential,

$$\mathbf{A}^\xi = (A_x^\xi, A_y^\xi) = \frac{\hbar}{e} (p_x^\xi - p_{x0}^\xi, p_y^\xi - p_{y0}^\xi), \quad (\text{B4})$$

which results in an effective magnetic field

$$B^\xi = \frac{\partial A_y^\xi}{\partial x} - \frac{\partial A_x^\xi}{\partial y} = \frac{\hbar}{e} \left(\frac{\partial p_y^\xi}{\partial x} - \frac{\partial p_x^\xi}{\partial y} \right). \quad (\text{B5})$$

Using the definition of \mathbf{v}_1 and \mathbf{v}_2 and the constraint $p + q + r = N$ (for the a sublattice), we obtain,

$$\begin{aligned} p &= \frac{Nu - x}{3u} - \frac{y}{\sqrt{3}u}, \\ q &= \frac{Nu - x}{3u} + \frac{y}{\sqrt{3}u}, \\ r &= \frac{N}{3} + \frac{2x}{3u}. \end{aligned} \quad (\text{B6})$$

Substituting Eqs. (B2), (B3), and (B6) in Eq. (B5), we obtain

$$B^\xi = -\xi \frac{2\hbar}{Neu^2} \frac{1}{\sqrt{1 - 4r^2/u^2N^2}} = -\xi \frac{B_0}{\sqrt{1 - r^2/R^2}}. \quad (\text{B7})$$

APPENDIX C: RELATION BETWEEN THE COHERENT WAVE PACKET IN THE ZEROth LANDAU LEVEL AND THE PSEUDO-SPIN COHERENT STATE

The pseudo-spin coherent state denoted by two angles on the Bloch sphere is

$$|\theta, \phi\rangle = \sum_{k=0}^N \sqrt{\frac{N!}{(N-k)!k!}} e^{ik\phi} \cos^{N-k} \frac{\theta}{2} \sin^k \frac{\theta}{2} |\psi_{0,2(j-k)}\rangle. \quad (\text{C1})$$

Using Eqs. (C1) and (A5) we can obtain the corresponding wavefunction $\psi_{\theta, \phi}(\mathbf{r})$. The expectation value of the angular momentum is determined by the orientation (θ, ϕ) as $\langle J_x \rangle \hat{x} + \langle J_y \rangle \hat{y} + \langle J_z \rangle \hat{z} = j \sin \theta \cos \phi \hat{x} + j \sin \theta \sin \phi \hat{y} + j \cos \theta \hat{z}$. According to Eqs. (D3a) and (D3b), the corresponding expectation value of the position in the Fock-state lattice is obtained

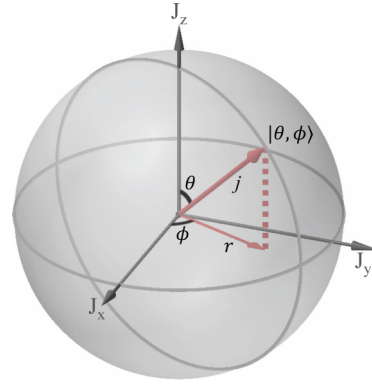


FIG. 5. The pseudo-spin coherent state $|\theta, \phi\rangle$ on the Bloch sphere with the total angular momentum $j = N/2$. The equator is the in-circle of the Fock-state lattice with a radius $R = uN/2$.

as (see Fig. 5),

$$\begin{aligned} \langle X \rangle \hat{x} + \langle Y \rangle \hat{y} &= u \langle J_x \rangle \hat{x} + u \langle J_y \rangle \hat{y} \\ &= ju \sin \theta \cos \phi \hat{x} + \sin \theta \sin \phi \hat{y} \\ &= R \sin \theta \cos \phi \hat{x} + R \sin \theta \sin \phi \hat{y}. \end{aligned} \quad (\text{C2})$$

APPENDIX D: THE GUIDING CENTER, MECHANICAL MOMENTUM, AND THEIR COMMUTATION RELATIONS

The position operators of the lattice are defined as

$$\begin{aligned} x &\rightarrow u(2c_3^\dagger c_3 - c_1^\dagger c_1 - c_2^\dagger c_2)/2, \\ y &\rightarrow u(c_2^\dagger c_2 - c_1^\dagger c_1)\sqrt{3}/2. \end{aligned} \quad (\text{D1})$$

The guiding-center coordinates are defined by

$$X = x - \frac{1}{eB^\xi} P_y, \quad Y = y + \frac{1}{eB^\xi} P_x, \quad (\text{D2})$$

where X, Y are the guiding center operators. The position operators are rewritten in d modes by applying the transformation $(c_1^\dagger, c_2^\dagger, c_3^\dagger)^T = U^{-1}(d_0^\dagger, d_+^\dagger, d_-^\dagger)^T$,

$$\begin{aligned} x &\rightarrow \frac{u}{2}(d_+^\dagger d_- + d_-^\dagger d_+) + \frac{u}{2}[d_0^\dagger(d_+ + d_-) + (d_+^\dagger + d_-^\dagger)d_0] \\ &\rightarrow X + \frac{1}{eB^\xi} P_y, \end{aligned} \quad (\text{D3a})$$

$$\begin{aligned} y &\rightarrow \frac{ui}{2}(d_+^\dagger d_+ - d_+^\dagger d_-) + \frac{ui}{2}[d_0^\dagger(d_- - d_+) + (d_+^\dagger - d_-^\dagger)d_0] \\ &\rightarrow Y - \frac{1}{eB^\xi} P_x, \end{aligned} \quad (\text{D3b})$$

where $X \rightarrow uJ_x, Y \rightarrow uJ_y$ are the coordinates of the guiding center and B^ξ is the magnetic field. Since the Hamiltonian only contains d_0 and d_0^\dagger operators, the coordinates of the guiding center is obtained by dropping these operators in x and y . The commutation relation is

$$[X, Y] \rightarrow iu^2 J_z. \quad (\text{D4})$$

The covariant momentum operators are the terms including d_0 and d_0^\dagger ,

$$\begin{aligned} P_x &\rightarrow \frac{eB^\xi u}{2} i[d_0^\dagger(d_+ - d_-) - (d_+^\dagger - d_-^\dagger)d_0], \\ P_y &\rightarrow \frac{eB^\xi u}{2} [d_0^\dagger(d_+ + d_-) + (d_+^\dagger + d_-^\dagger)d_0]. \end{aligned} \quad (\text{D5})$$

The commutation relation between P_x and P_y is

$$[P_x, P_y] \rightarrow -i(ueB^z)^2 J_z. \quad (\text{D6})$$

We also have

$$[X, P_x] = -[Y, P_y] \rightarrow \frac{ieB^z u^2}{4} [d_0(d_+^\dagger - d_-^\dagger) + d_0^\dagger(d_+ - d_-)]. \quad (\text{D7})$$

When the electric field is small and there is only intraband dynamics, we can regard $[X, P_x] = -[Y, P_y] \approx 0$.

-
- [1] N. R. Cooper, J. Dalibard, and I. B. Spielman, Topological bands for ultracold atoms, *Rev. Mod. Phys.* **91**, 015005 (2019).
- [2] L. Yuan, Q. Lin, M. Xiao, and S. Fan, Synthetic dimension in photonics, *Optica* **5**, 1396 (2018).
- [3] T. Ozawa and H. M. Price, Topological quantum matter in synthetic dimensions, *Nat. Rev. Phys.* **1**, 349 (2019).
- [4] D.-W. Wang, R.-B. Liu, S.-Y. Zhu, and M. O. Scully, Superradiance Lattices, *Phys. Rev. Lett.* **114**, 043602 (2015).
- [5] D.-W. Wang, H. Cai, L. Yuan, S.-Y. Zhu, and R.-B. Liu, Topological phase transitions in superradiance lattices, *Optica* **2**, 712 (2015).
- [6] D. W. Wang, H. Cai, R. B. Liu, and M. O. Scully, Mesoscopic Superposition States Generated by Synthetic Spin-Orbit Interaction in Fock-State Lattices, *Phys. Rev. Lett.* **116**, 220502 (2016).
- [7] H. Cai and D. W. Wang, Topological phases of quantized light, *Nat. Sci. Rev.* **8**, nwaa196 (2020).
- [8] W. P. Su, J. R. Schrieffer, and A. J. Heeger, Solitons in Polyacetylene, *Phys. Rev. Lett.* **42**, 1698 (1979).
- [9] H. Suzuura and T. Ando, Phonons and electron-phonon scattering, *Phys. Rev. B* **65**, 235412 (2002).
- [10] S. V. Morozov, K. S. Novoselov, M. I. Katsnelson, F. Schedin, L. A. Ponomarenko, D. Jiang, and A. K. Geim, Strong Suppression of Weak Localization in Graphene, *Phys. Rev. Lett.* **97**, 016801 (2006).
- [11] A. F. Morpurgo and F. Guinea, Intervalley Scattering, Long-Range Disorder, and Effective Time-Reversal Symmetry Breaking in Graphene, *Phys. Rev. Lett.* **97**, 196804 (2006).
- [12] J. L. Mañes, Symmetry-based approach to electron-phonon interactions in graphene, *Phys. Rev. B* **76**, 045430 (2007).
- [13] V. M. Pereira, A. H. Castro Neto, and N. M. R. Peres, Tight-binding approach to uniaxial strain in graphene, *Phys. Rev. B* **80**, 045401 (2009).
- [14] D. I. Pikulin, A. Chen, and M. Franz, Chiral Anomaly from Strain-Induced Gauge Fields in Dirac and Weyl Semimetals, *Phys. Rev. X* **6**, 041021 (2016).
- [15] S. Guan, Z. M. Yu, Y. Liu, G. B. Liu, L. Dong, Y. Lu, Y. Yao, and S. A. Yang, Artificial gravity field, astrophysical analogues, and topological phase transitions in strained topological semimetals, *npj Quant. Mater.* **2**, 23 (2017).
- [16] H. Jia, R. Zhang, W. Gao, Q. Guo, B. Yang, J. Hu, Y. Bi, Y. Xiang, C. Liu, and S. Zhang, Observation of chiral zero mode in inhomogeneous three-dimensional Weyl metamaterials, *Science* **363**, 148 (2019).
- [17] A. H. Castro Neto, F. Guinea, N. M. R. Peres, K. S. Novoselov, and A. K. Geim, The electronic properties of graphene, *Rev. Mod. Phys.* **81**, 109 (2009).
- [18] M. O. Goerbig, Electronic properties of graphene in a strong magnetic field, *Rev. Mod. Phys.* **83**, 1193 (2011).
- [19] F. Guinea, M. I. Katsnelson, and A. K. Geim, Energy gaps and a zero-field quantum hall effect in graphene by strain engineering, *Nat. Phys.* **6**, 30 (2010).
- [20] N. Levy, S. A. Burke, K. L. Meaker, M. Panlasigui, A. Zettl, F. Guinea, A. H. Castro Neto, and M. F. Crommie, Strain-induced pseudo-magnetic fields greater than 300 tesla in graphene nanobubbles, *Science* **329**, 544 (2010).
- [21] W. Yan, W. Y. He, Z. D. Chu, M. Liu, L. Meng, R. F. Dou, Y. Zhang, Z. Liu, J. C. Nie, and L. He, Strain and curvature induced evolution of electronic band structures in twisted graphene bilayer, *Nat. Commun.* **4**, 2159 (2013).
- [22] K. K. Gomes, W. Mar, W. Ko, F. Guinea, and H. C. Manoharan, Designer Dirac fermions and topological phases in molecular graphene, *Nature (London)* **483**, 306 (2012).
- [23] B. Tian, M. Endres, and D. Pekker, Landau Levels in Strained Optical Lattices, *Phys. Rev. Lett.* **115**, 236803 (2015).
- [24] M. C. Rechtsman, J. M. Zeuner, Y. Plotnik, Y. Lumer, D. Podolsky, F. Dreisow, S. Nolte, M. Segev, and A. Szameit, Photonic Floquet topological insulators, *Nature (London)* **496**, 196 (2013).
- [25] Z. Yang, F. Gao, Y. Yang, and B. Zhang, Strain-Induced Gauge Field and Landau Levels in Acoustic Structures, *Phys. Rev. Lett.* **118**, 194301 (2017).
- [26] X. Wen, C. Qiu, Y. Qi, L. Ye, M. Ke, F. Zhang, and Z. Liu, Acoustic Landau quantization and quantum-Hall-like edge states, *Nat. Phys.* **15**, 352 (2019).
- [27] F. Zhai, X. Zhao, K. Chang, and H. Q. Xu, Magnetic barrier on strained graphene: A possible valley filter, *Phys. Rev. B* **82**, 115442 (2010).
- [28] A. Chaves, L. Covaci, K. Yu. Rakhimov, G. A. Farias, and F. M. Peeters, Wave-packet dynamics and valley filter in strained graphene, *Phys. Rev. B* **82**, 205430 (2010).
- [29] J. R. Schaibley, H. Yu, G. Clark, P. Rivera, J. S. Ross, K. L. Seyler, W. Yao, and X. Xu, Valleytronics in 2D materials, *Nat. Rev. Mater.* **1**, 16055 (2016).
- [30] A. J. Pearce, E. Mariani, and G. Burkard, Tight-binding approach to strain and curvature in monolayer transition-metal dichalcogenides, *Phys. Rev. B* **94**, 155416 (2016).
- [31] D. Zhai and W. Yao, Layer Pseudospin Dynamics and Genuine Non-Abelian Berry Phase in Inhomogeneously Strained Moiré Pattern, *Phys. Rev. Lett.* **125**, 266404 (2020).
- [32] É. Lantagne-Hurtubise, X. X. Zhang, and M. Franz, Dispersive Landau levels and valley currents in strained graphene nanoribbons, *Phys. Rev. B* **101**, 085423 (2020).
- [33] D. Xiao, W. Yao, and Q. Niu, Valley-Contrasting Physics in Graphene: Magnetic Moment and Topological Transport, *Phys. Rev. Lett.* **99**, 236809 (2007).
- [34] W. Yao, D. Xiao, and Q. Niu, Valley-dependent optoelectronics from inversion symmetry breaking, *Phys. Rev. B* **77**, 235406 (2008).

- [35] D. Xiao, G. B. Liu, W. Feng, X. Xu, and W. Yao, Coupled Spin and Valley Physics in Monolayers of MoS₂ and Other Group-VI Dichalcogenides, *Phys. Rev. Lett.* **108**, 196802 (2012).
- [36] F. D. M. Haldane, Model for a Quantum Hall Effect without Landau Levels: Condensed-Matter Realization of the Parity Anomaly, *Phys. Rev. Lett.* **61**, 2015 (1988).
- [37] Y. Aharonov and D. Bohm, Significance of electromagnetic potentials in the quantum theory, *Phys. Rev.* **115**, 485 (1959).
- [38] M. V. Berry, Quantal phase factors accompanying adiabatic changes, *Proc. R. Soc. London* **392**, 45 (1984).
- [39] G. Jotzu, M. Messer, R. Desbuquois, M. Lebrat, T. Uehlinger, D. Greif, and T. Esslinger, Experimental realization of the topological Haldane model, *Nature* **515**, 237 (2014).
- [40] Y. H. Ho, E. V. Castro, and M. A. Cazalilla, Haldane model under nonuniform strain, *Phys. Rev. B* **96**, 155446 (2017).
- [41] S. Rachel, I. Gothel, D. P. Arovas, and M. Vojta, Strain-Induced Landau Levels in Arbitrary Dimensions with an Exact Spectrum, *Phys. Rev. Lett.* **117**, 266801 (2016).
- [42] R. Ilan, A. G. Grushin, and I. Pikulin, Pseudo-electromagnetic fields in 3D topological semimetals, *Nat. Rev. Phys.* **2**, 29 (2020).
- [43] Y. Li and C. Wu, High-Dimensional Topological Insulators with Quaternionic Analytic Landau Levels, *Phys. Rev. Lett.* **110**, 216802 (2013).
- [44] Y. Li, K. Intriligator, Y. Yu, and C. Wu, Isotropic Landau levels of Dirac fermions in high dimensions, *Phys. Rev. B* **85**, 085132 (2012).
- [45] E. T. Jaynes and F. W. Cummings, Comparison of quantum and semiclassical radiation theories with application to the beam maser, *Proc. IEEE* **51**, 89 (1963).
- [46] F. De Juan, M. Sturla, and M. A. H. Vozmediano, Space Dependent Fermi Velocity in Strained Graphene, *Phys. Rev. Lett.* **108**, 227205 (2012).
- [47] I. M. Lifshitz, Anomalies of electron characteristics of a metal in the high pressure region, *J. Exptl. Theoret. Phys. (U.S.S.R.)* **38**, 1569 (1960).
- [48] J. J. Sakurai and J. Napolitano, *Modern Quantum Mechanics*, 2nd ed. (Cambridge University Press, Cambridge, 2017).
- [49] E. Layton, Y. Huang, and S. I. Chu, Cyclic quantum evolution and Aharonov-Anandan geometric phases in SU(2) spin-coherent states, *Phys. Rev. A* **41**, 42 (1990).
- [50] G. S. Agarwal, R. R. Puri, and R. P. Singh, Atomic Schrödinger cat states, *Phys. Rev. A* **56**, 2249 (1997).
- [51] D. J. Thouless, M. Kohmoto, M. P. Nightingale, and M. den Nijs, Quantized Hall Conductance in a Two-Dimensional Periodic Potential, *Phys. Rev. Lett.* **49**, 405 (1982).
- [52] D.-W. Wang, C. Song, W. Feng, H. Cai, D. Xu, H. Deng, H. Li, D. Zheng, X. Zhu, H. Wang *et al.*, Synthesis of antisymmetric spin exchange interaction and chiral spin clusters in superconducting circuits, *Nat. Phys.* **15**, 382 (2019).
- [53] Z. Wang, H. Li, W. Feng, X. Song, C. Song, W. Liu, Q. Guo, X. Zhang, H. Dong, D. Zheng, H. Wang, and D.-W. Wang, Controllable Switching between Superradiant and Subradiant States in a 10-qubit Superconducting Circuit, *Phys. Rev. Lett.* **124**, 013601 (2020).
- [54] W. Ren, W. Liu, C. Song, H. Li, Q. Guo, Z. Wang, D. Zheng, G. S. Agarwal, M. O. Scully, S.-Y. Zhu, H. Wang, and D.-W. Wang, Simultaneous Excitation of Two Noninteracting Atoms with Time-Frequency Correlated Photon Pairs in a Superconducting Circuit, *Phys. Rev. Lett.* **125**, 133601 (2020).
- [55] J. Yuan, C. Xu, H. Cai, and D.-W. Wang, Gap-protected transfer of topological defect states in photonic lattices, *APL Photonics* **6**, 030803 (2021).
- [56] W. Liu, W. Feng, W. Ren, D.-W. Wang, and H. Wang, Synthesizing three-body interaction of spin chirality with superconducting qubits, *Appl. Phys. Lett.* **116**, 114001 (2020).